Letter

Enhanced ferromagnetism in an artificially stretched lattice in quasi-two-dimensional $Cr_2Ge_2Te_6$

Hiroshi Idzuchi,[1,2,3,4,*,†] Andres E. Llacsahuanga Allcca,[3,5,*] Anh Khoa Augustin Lu,[6,7] Mitsuhiro Saito,[1,8] Subhadip Das,[9] John F. Ribeiro,[10] Michel Houssa,[11] Ruishen Meng,[11] Kazutoshi Inoue,[1] Xing-Chen Pan,[1] Katsumi Tanigaki,[1,12] Yuichi Ikuhara,[1,8] Takeshi Nakanishi,[6] and Yong P. Chen[1,2,3,5,9,10,‡]

[1]*WPI Advanced Institute for Materials Research (AIMR), Tohoku University, Sendai 980-8577, Japan*
[2]*Center for Science and Innovation in Spintronics (CSIS), Tohoku University, Sendai 980-8577, Japan*
[3]*Department of Physics and Astronomy, Purdue University, West Lafayette, Indiana 47907, USA*
[4]*Department of Physics, The University of Tokyo, Bunkyo-ku, Tokyo 113-0033, Japan*
[5]*Birck Nanotechnology Center and Purdue Quantum Science and Engineering Institute, Purdue University, West Lafayette, Indiana 47907, USA*
[6]*Mathematics for Advanced Materials Open Innovation Laboratory, National Institute of Advanced Industrial Science and Technology, Sendai 980-8577, Japan*
[7]*Research Center for Materials Nanoarchitectonics, National Institute for Materials Science, Tsukuba 305-0044, Japan*
[8]*Institute of Engineering Innovation, The University of Tokyo, Tokyo 113-8656, Japan*
[9]*Institute of Physics and Astronomy and Villum Centers for Dirac Materials and for Hybrid Quantum Materials and Devices, Aarhus University, 8000 Aarhus-C, Denmark*
[10]*School of Electrical and Computer Engineering, Purdue University, West Lafayette, Indiana 47907, USA*
[11]*Department of Physics and Astronomy, Katholieke Universiteit Leuven, 3001 Leuven, Belgium*
[12]*Beijing Academy of Quantum Information and Sciences, Beijing 100193, China*

(Received 3 January 2023; revised 23 January 2024; accepted 15 November 2024; published 7 January 2025)

Crystal lattice is key in understanding magnetic interactions between atoms in solids. As the effective control of the lattice via tensile stress is limited, there are only a few demonstrations of controlling magnetic properties by expanding the lattice. This study reveals a clear correlation between enhanced magnetism, where Curie temperature (T_C) is doubled from ∼60 to ∼120 K, and lattice expansion in prototypical van der Waals magnet $Cr_2Ge_2Te_6$ with sputtered dielectric overlayers NiO and MgO. We ascribe the mechanism of this T_C increase to a change in exchange interactions induced by strain, studied by several experimental probes and computational approaches.

DOI: 10.1103/PhysRevB.111.L020402

Magnetic interactions at the atomic level play a central role in magnetism. The recent rise of two-dimensional van der Waals (vdW) magnetic materials offers the possibility to study magnetic interactions thanks to their high crystallinity, tunability, and the possibility to study various thicknesses [1,2], where the lattice characteristics can be easily accessed by several probes with spatial resolution such as scanning probes and Raman spectroscopy [3–5]. One of the most important indications of magnetic interactions is the Curie temperature (T_C). With the practical motivation to increase T_C, the relation between magnetic interactions and T_C has been widely studied in vdW magnets. For example, the change in magnetic interactions with the electronic structure and carrier concentration was studied by electric gating (in particular in the structure of a field-effect transistor), which changes the hysteresis curve for a localized magnetic system of $Cr_2Ge_2Te_6$ without any significant change in T_C, whereas the T_C increases from 205 K to above room temperature in the case of an itinerant magnetic system of Fe_3GeTe_2 in a similar structure [6,7]. Historically, external pressure has been used for tailoring the lattice parameter of magnetic systems. This approach was applied to both itinerant and localized magnetic systems, but it was found that T_C of prototypical ferromagnet CrI_3 only slightly increased from 44 to 48 K [8]. While an external pressure could be used for shrinking the lattice, it cannot be used for an expansion of the lattice and the studies in small-size samples are rather limited [9]. Previously, some of us reported an increased T_C in $Cr_2Ge_2Te_6$/NiO heterostructure but its mechanism including the effect of the strain was left unclear [10]. In this Letter, we present a clear correlation between enhanced magnetism in $Cr_2Ge_2Te_6$/NiO and $Cr_2Ge_2Te_6$/MgO heterostructures and the tensile strain from wrinkle formation, where we can achieve nearly twice the T_C of bulk and as-cleaved $Cr_2Ge_2Te_6$. Such a heterointerface provides a different tuning knob for controlling the order parameters by expanding the lattice, which cannot be accessed by conventional schemes such as frequently used pressure cells.

When an in-plane tensile force is applied to some but not all layers of a multilayer system [Fig. 1(a)], a wrinkle can form in the stretched part to conserve the total number of atoms [Fig. 1(b)]. Previous research indicates that biaxial strain can be induced in two-dimensional (2D) materials upon depositing oxide thin films, where the strain originates from

*These authors contributed equally to this work.
†Contact author: hiroshi.idzuchi@phys.u-tokyo.ac.jp
‡Contact author: yongchen@purdue.edu

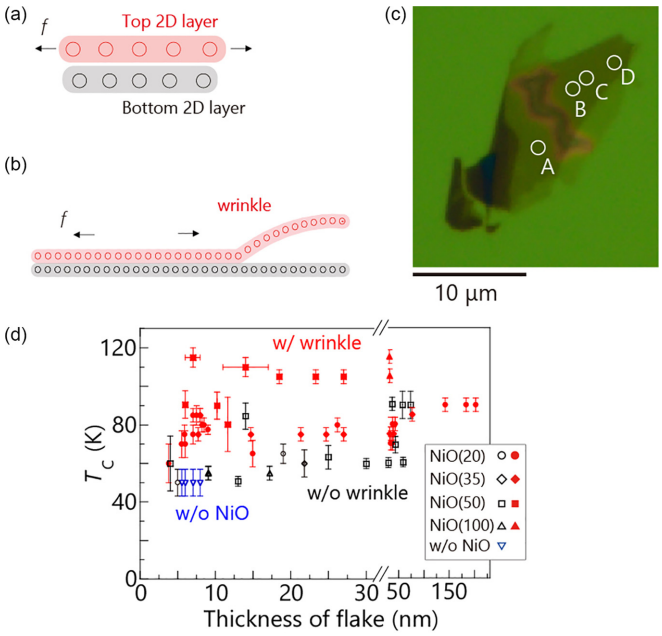

FIG. 1. Wrinkle formation in $Cr_2Ge_2Te_6$/NiO and impact on magnetic T_C. (a) Schematic mechanism to form wrinkle in 2D layers (focusing on two representative layers represented by red and black shaded regions). Each circle represents an atom. In the top layer, an in-plane tensile force f is applied and results in a lateral displacement of atoms from the original positions (indicated in the bottom layer in black). (b) In regions other than the part shown in (a), such as the right portion of this figure, accommodating the stretched lattice may induce a deformation of the layer (such as wrinkles), especially when the coupling to the adjacent layers is weak, which is the case in 2D materials. (c) Optical micrograph of a $Cr_2Ge_2Te_6$ flake with a 50-nm-thick NiO overlayer. Wrinkles appear as wavy patterns near the center of the flake. Several representative positions ae marked as circles (A, B, C, and D). (d) Curie temperatures of $Cr_2Ge_2Te_6$ flakes of different thicknesses (bottom axis), with (data in red and black) and without (blue) NiO layer. The results for flakes with (without) wrinkles are indicated by closed red (open black) symbols. The symbols reflect the NiO thickness: 20 nm (circle), 35 nm (diamond), 50 nm (rectangle), and 100 nm (triangle).

the attempt to relax the residual stress of the oxide film [11], suggesting that wrinkle formation or buckling delamination [Fig. 1(b)] may form with sufficiently strong strain. Such strain-induced deformations are observed in our 2D magnet $Cr_2Ge_2Te_6$ after sputtering NiO [a representative image is shown in Fig. 1(c), with more detailed characterizations shown in the Supplemental Material [12]]. We prepared our samples by mechanical exfoliation from a single crystal of $Cr_2Ge_2Te_6$ on a silicon substrate (with 285-nm SiO_2). A NiO layer with a thickness of 20–100 nm was sputtered onto the substrate containing the exfoliated $Cr_2Ge_2Te_6$ flakes. Details of the sample preparation are described in the previous report [10]. The formation of wrinkles was commonly observed on $Cr_2Ge_2Te_6$ flakes [10]. For thick $Cr_2Ge_2Te_6$ samples, the portion close to the $Cr_2Ge_2Te_6$/NiO interface deforms and delaminates from the rest of the sample. We note that graphite and MoS_2 [23,24] are just a few examples of other 2D/vdW materials in which wrinkle structures (formed during growth or other processes) have been noted. In contrast to the method to strain an entire flake on a flexible substrate by deforming the substrate [25], our method involved an overlayer (NiO) that induces strain (a change in lattice spacing) particularly when the sample showed a wrinkled structure. We note that such a wrinkled structure resulting in a curved section of the 2D ferromagnet can break the inversion symmetry and possibly lead to a strong Dzyaloshinskii-Moriya interaction and noncollinear spin configurations [26].

The magnetic properties of the $Cr_2Ge_2Te_6$/NiO heterostructure were characterized by the magneto-optical Kerr effect (MOKE) measurements [12], which we used previously to report an enhanced ferromagnetic transition (Curie) temperature T_C. Figure 1(d) shows the T_C for three typical cases: two types of $Cr_2Ge_2Te_6$/NiO (flakes with and without wrinkles) and $Cr_2Ge_2Te_6$ without NiO layer. Flakes of $Cr_2Ge_2Te_6$/NiO with wrinkles exhibit higher T_C for various thicknesses, up to nearly twice the T_C of bare $Cr_2Ge_2Te_6$ without the NiO layer, while flakes of $Cr_2Ge_2Te_6$/NiO with no wrinkles tend to exhibit a T_C similar to the bare $Cr_2Ge_2Te_6$. While the increase in T_C for wrinkled $Cr_2Ge_2Te_6$/NiO has been reported in our previous work, the underlying mechanism and the physical effects of the wrinkle structure were unknown at that time [10]. This will be the focus of this work.

First, the spatial variation of Raman and MOKE characteristics near the wrinkles are examined. Figures 2(a) and 2(b) show the Raman spectra with five characteristic peaks in the 80–320 cm^{-1} range measured at room temperature [4] at four different positions of a representative flake [optical micrograph and the positions are shown in Fig. 1(c)]. The positions of the peaks in the Raman spectrum change with the position in the flake, even with the same $Cr_2Ge_2Te_6$ thickness, and this can be explained by a position-dependent strain. Note that we have discussed the hysteresis at the same position before and after forming NiO in the previous report [10]. The peak near 235 cm^{-1} (110 cm^{-1}) is ascribed to an (two) in-plane vibration mode(s), whereas the other three peaks are assigned to other types of vibrations, i.e., an out-of-plane mode and a combination of the two modes [27]. The MOKE measurement at the same positions [Fig. 2(c)] indicates that ferromagnetic T_C also varies with the position. The Raman-peak position map [Fig. 2(d)] shows that the peak position varies with the distance from a wrinkle in the flake. A correlation between the Raman peak position and T_C indicates that T_C becomes higher when the Raman peak shifts to lower wave numbers. Such a Raman peak shift towards lower wave numbers indicates tensile strain, as reported in the pressure experiments [28,29] and in our bending experiments where a tensile force was applied by deforming the flexible substrate onto which the flake was placed [12].

Next, we address the general trend in the correlation between wrinkles, strain, and magnetism based on observations from many samples. We noticed that the wrinkle formation, while it does not always happen in every exfoliated $Cr_2Ge_2Te_6$ flake, can occur for flakes with all ranges of thicknesses up to the bulk limit [12]. The wrinkle formation was also occasionally observed in flakes during the cooling process. Despite such a varied wrinkle behavior, the strain was examined by studying 57 positions on 27 flakes with and without NiO overlayer, focusing on thin flakes (<15 nm) for the Raman to properly characterize the strained top layers

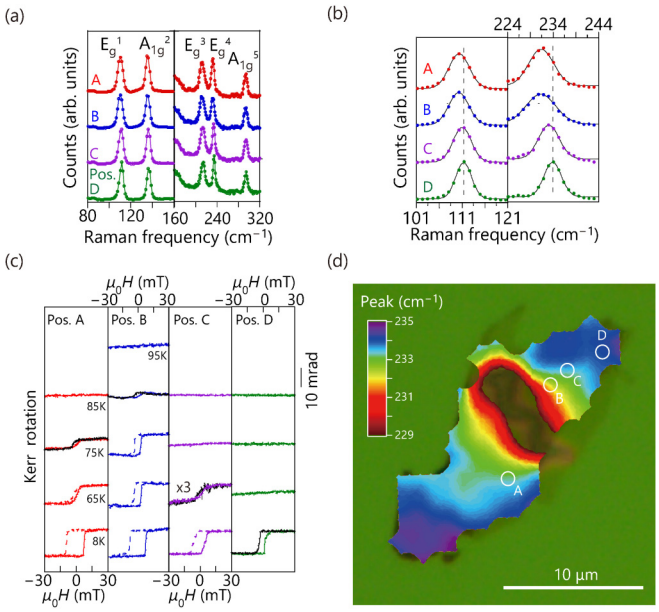

FIG. 2. Raman spectra and magnetic properties of a wrinkled flake. (a) Raman spectra of the flake at positions A (red), B (blue), C (purple), and D (green) shown in Fig. 1(c), in the 80–320 cm^{-1} range. According to theoretical calculations, five peaks, E_g^1, E_g^3, E_g^4, (A_{1g}^2, A_{1g}^5), are expected in this frequency range, three (two) of which are nearly doubly degenerated (nondegenerated) modes. (b) Zoomed-in spectra from (a) around the E_g^1 (left) and E_g^4 (right) peaks (vertical dotted lines mark the Raman peak for position D). The solid lines connecting the data points represent fitted curves. (c) Kerr rotation at positions A (red), B (blue), C (purple), and D (green), from left to right. The hysteresis curves for magnetic fields (applied perpendicular to the sample plane) are presented for several temperatures (8, 65, 75, 85, and 95 K). The curves are shifted vertically for clarity. Sweeps from positive to negative fields (or reverse) are indicated by dotted or black (or solid) lines. The vertical scale bar indicates 10 mrad. (d) Spatial distribution of the Raman E_g^4 peak position (plotted as color, except the green background color outside the flake). The color and contour plot were generated by interpolating values measured every 0.8 μm.

[12]. The Raman peak position is distinctively lower, indicating tensile strain, for the flakes with wrinkles than for those without wrinkles regardless of the presence of a NiO layer [Fig. 3(a)]. The strain-induced shifts of two Raman modes should correlate, which is clearly seen in Fig. 3(a) for E_g^1 (∼111–112 cm^{-1}) and E_g^4 (∼234–235 cm^{-1}) peaks [see Fig. S4 of the Supplemental Material for the A_{1g}^2 (∼137 cm^{-1}) mode [12]]. To estimate the strain (lattice constant change) from the Raman shift, we note that a 1% lattice constant shrinkage, based on pressure cell experiment, reportedly gives a shift of about ∼−4 cm^{-1} for the E_g^1 peak around 110 cm^{-1} [29]. The Raman peak shift per strain, assuming isotropic shrinking and therefore triaxial strain, for such a peak was extracted to be ∼−1.3 cm^{-1}/%, which is also consistent with our bending experiment. The negative sign between wave number and strain (meaning lattice expansion gives redshift of Raman peak) is consistent with the results obtained from first-principles studies on monolayer $Cr_2Ge_2Te_6$ [27]. We also performed polarized Raman experiments to evaluate the in-plane anisotropy and found it to be small [12], so we used data from unpolarized Raman measurements for most of our analysis unless otherwise noted. We studied the correlation between T_C and Raman peaks on four flakes focusing on two in-plane Raman modes [Fig. 3(b)], and extracted an approximate linear correlation of ∼−20 K/cm^{-1} (converting to a rate of change of T_C to strain ∼26 K/%).

Magnetism in $Cr_2Ge_2Te_6$ mainly relies on the interactions between Cr atoms, which form a quasi-2D honeycomb lattice. Such interactions have been studied previously in $MCrS_2$ systems (M is a monovalent metal among Li, Na, K, Ag, and Au) [30,31]. Specifically, three unpaired electrons from Cr form triplet t_{2g} orbitals with a lower energy than doublet e_g states. The direct overlap between different t_{2g} orbitals of neighboring Cr ions gives rise to strong antiferromagnetic (AFM) exchange interactions, which strongly depend on and decrease with increasing Cr-Cr distance. This competes with ferromagnetic (FM) interactions that are caused by virtual hopping from the occupied t_{2g} shell of one Cr to the empty e_g

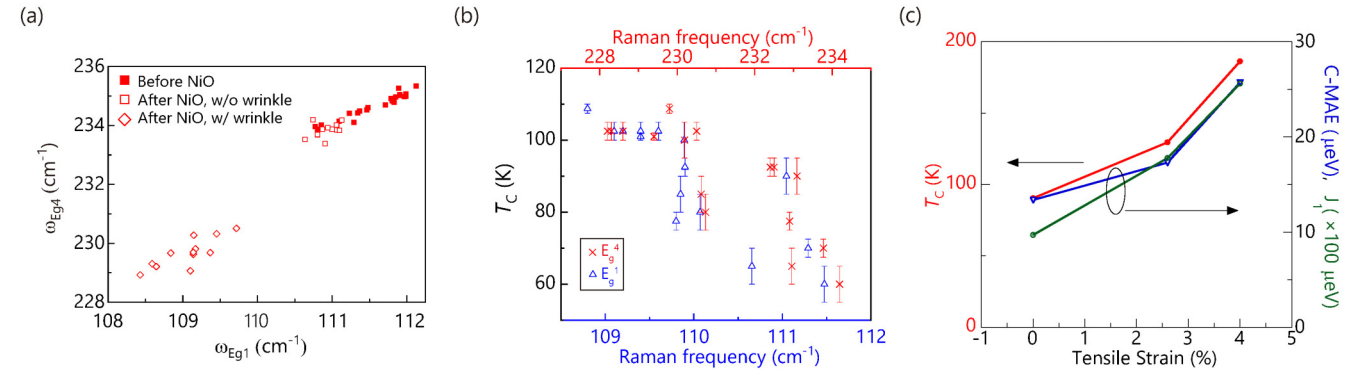

FIG. 3. Correlation between tensile strain and enhanced magnetism. (a) The correlation between peak positions of two in-plane Raman modes (E_g^4 vs E_g^1) for $Cr_2Ge_2Te_6$. Samples (after) before depositing NiO which do not show wrinkles are indicated as (open) solid rectangles. Samples after depositing NiO which show wrinkles are indicated by diamonds. (b) Relationship between the measured Curie temperature (T_C) and the two in-plane Raman modes peaks positions [top (E_g^4) and bottom (E_g^1) axes] for $Cr_2Ge_2Te_6$ samples with a NiO overlayer. (c) Curie temperature T_C (red filled circle), crystalline magnetoanisotropy energy C-MAE (blue triangle), and first exchange coupling J_1 (green empty circle) with respect to the in-plane tensile strain, from DFT calculations.

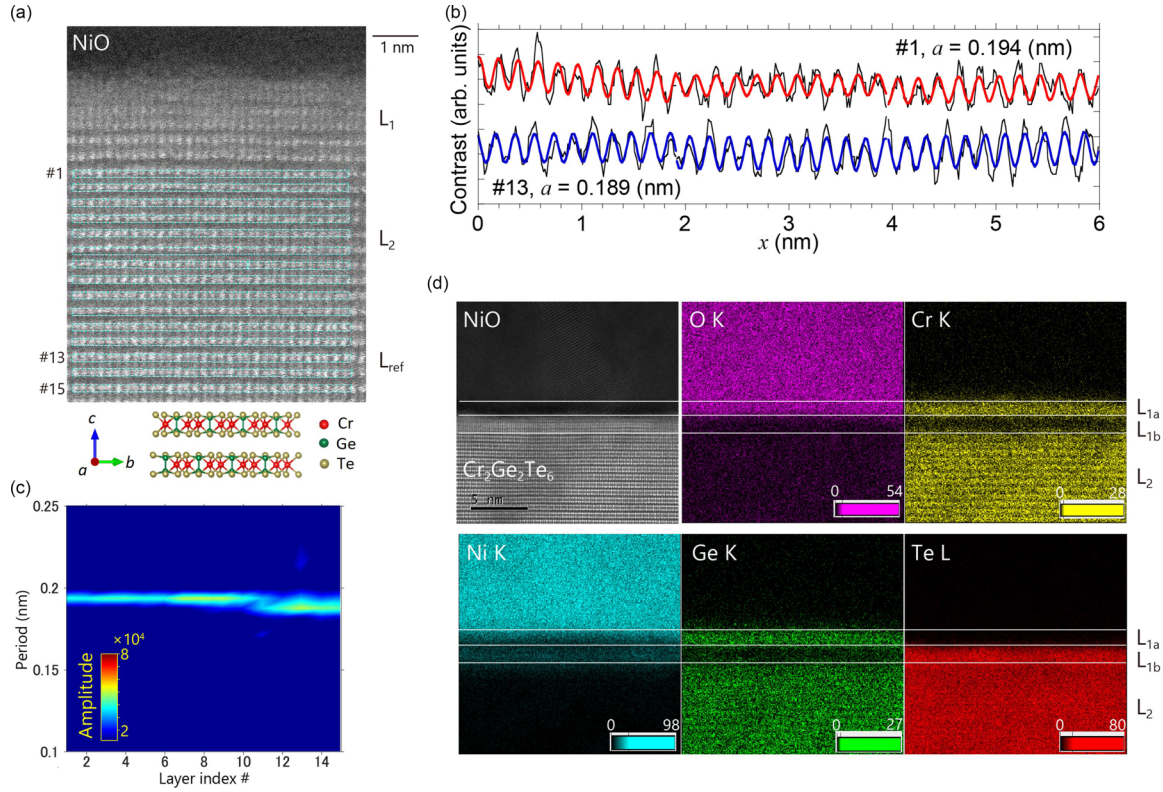

FIG. 4. STEM image and tensile strain in $Cr_2Ge_2Te_6$ layers. (a) Top: cross-section STEM image of a $Cr_2Ge_2Te_6$/NiO. The upper dark region indicates the NiO overlayer. In the lower region, well-defined flat layered patterns indicate the $Cr_2Ge_2Te_6$ layers [each layer highlighted by blue dashed rectangles, highlighting the area to count the contrast in (b) and (c)]. These layers are individually numbered (1, 2, …15). Between these and NiO, there is a region (labeled as L_1) with less flat layers and less sharp contrast. L_2 (L_{ref}) represents layers 1–10 ($n > 12$). The image was taken at the position ∼1 μm apart from the center of the wrinkle (not on the wrinkle itself). Bottom: atomic structure of $Cr_2Ge_2Te_6$ generated with VESTA [36], where the b axis direction (the horizontal direction in the STEM image above) is the zigzag direction. (b) The contrast variation with lateral position in layers 1 and 13 shown in (a). Red and blue curves show the fitting with the sine function (periods 0.194 and 0.189 nm). (c) Fourier transform (see Supplemental Material [12] for more details) of the highlighted region in (a). (d) STEM Energy Dispersive X-ray Spectroscopy mappings for O, Cr, Ni, Ge, and Te atoms with a scale bar of 5 nm. First panel shows a STEM image for the area. At the interface, there is a region showing intermixing, labeled as L_{1a} and L_{1b}, together corresponding to L_1 in (a).

shells of another Cr. This explains why the AFM (FM) nature is more pronounced in small (large) M in $MCrS_2$ compounds. In $Cr_2Ge_2Te_6$, we expect that the increase in Cr-Cr distance reduces the AFM exchange interaction, resulting in the net increase of the FM strength. The increased FM interaction in the stretched lattice is further confirmed by density functional theory (DFT) calculation and Monte Carlo simulations, as shown in Fig. 3(c). As tensile strain increases, the net ferromagnetic exchange energy thus T_C and the magnetoanisotropy increase [12]. Although similar calculations were previously reported in the atomically thin limit [27,32,33], we computed the increase of T_C for both the case of an atomically thin limit [12] and thick flake, the latter corresponding to the configuration of our experiment. Notably, for small strain values, a tensile strain of 1% leads to an increase in T_C of ≈17% (from 90 to 105 K) in reasonable agreement with the experimental data. It is interesting to note that in Fe_3GeTe_2, T_C is reported to increase from 180 to 210 K with strain, but the mechanism is considered to be more related to spin-orbit coupling [34].

The strain in a $Cr_2Ge_2Te_6$/NiO ($t_{NiO} = 50$ nm) heterostructure was further characterized by cross-sectional scanning transmission electron microscopy (STEM) [35]. Figure 4(a) displays a black-and-white contrast view, with electrons scattering from the $Cr_2Ge_2Te_6$ layers in the direction along the crystal axis perpendicular to the zigzag direction of Cr-Ge-Cr. A representative trace of the contrast gives a period of ≈0.19 nm [Figs. 4(b) and 4(c) [12]], in good agreement with the previous reported value for the Te-Te distance in $Cr_2Ge_2Te_6$ crystal (0.197 nm [30]). Interestingly, the $Cr_2Ge_2Te_6$ layers located near the $Cr_2Ge_2Te_6$/NiO interface (L_2 region) have a larger period (0.194 nm) than those located deeper and further away from the interface (0.189 nm). Such a larger period is also visible in the Fourier transformed image [12] based on the contrast of each layer [Fig. 4(c); note that the spatial frequency has been converted to period], further indicating the characteristic thickness of the stretched region (L_2) ≈10 layers [7 nm, not including the regions that do not show the periodic contrast (L_1 region)]. Within the thickness (∼27 nm) of $Cr_2Ge_2Te_6$ on SiO_2/Si in this specimen, apart from the layers in (L_1) region and the first 12 layers in (L_2) region, the rest of the layers (reference region) towards SiO_2 showed no notable change in the in-plane lattice parameters. An energy dispersive x-ray spectroscopy image of this specimen [Fig. 4(d)] shows that there are no notable deviations from stoichiometry in the L_2 region. However, at the same time, in line scans we notice that a small amount of Ni atoms

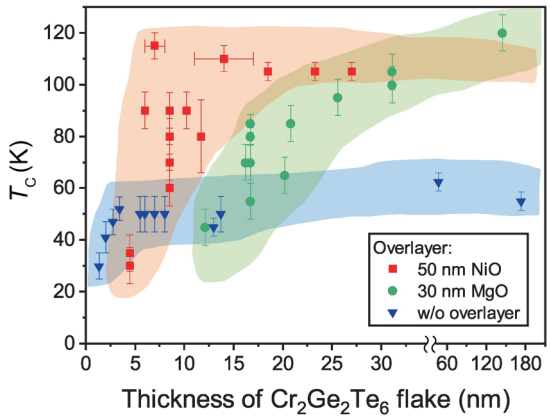

FIG. 5. Curie temperature in $Cr_2Ge_2Te_6$, $Cr_2Ge_2Te_6$/NiO, and $Cr_2Ge_2Te_6$/MgO. Curie temperature of $Cr_2Ge_2Te_6$ flakes with wrinkles with 50-nm-thick NiO overlayer (red square) and 30-nm-thick MgO overlayer (green circle). Data without any overlayer (blue triangle) are from this study except for the four data points of thinnest samples [1]. The shaded regions are visual guides.

(∼1%) are substituted up to ∼10 nm in depth [which cannot be seen in the mapping in Fig. 4(d)]. Note that first-principles modeling of Ni substitution (Supplemental Material Fig. S7) show that wiggles or buckling appear as a consequence of structure relaxations.

Below we further elaborate on the origin of the enhanced magnetism, and address the T_C dependence on the thickness of $Cr_2Ge_2Te_6$ flake. As shown in Fig. 1(d), T_C is enhanced even in the bulk limit of $Cr_2Ge_2Te_6$. This is consistent with the limited probing depth of MOKE, and the lattice deformation being limited to the layers close to the surface (as characterized by STEM and expected for strain transferred from a top sputtered thin film). For the thin limit, $Cr_2Ge_2Te_6$ shows suppressed magnetism attributed to large thermal fluctuations on the 2D limit [1] and disorder. We note that NiO is an antiferromagnetic material, and we observed no ferromagnetism in NiO itself in our MOKE measurements. We replaced NiO with MgO and prepared some $Cr_2Ge_2Te_6$/MgO heterostructures. We observed the formation of similar wrinkle structures, similar Raman peak shifts close to the wrinkles, and also enhancement in both T_C (Fig. 5) and coercive field [12]. The increase of T_C with MgO was as high as with NiO overlayer (up to 120 K) for thicker $Cr_2Ge_2Te_6$ flakes. These observations suggest that the enhanced magnetism in $Cr_2Ge_2Te_6$/NiO is unlikely related to the antiferromagnetism of NiO or doping of magnetic element Ni. For $Cr_2Ge_2Te_6$/MgO, the T_C starts to decrease rapidly with decreasing $Cr_2Ge_2Te_6$ thickness below "the critical thickness" $t_C \sim 17$ nm, and MOKE hysteresis can no longer be observed for ∼12 nm or thinner. For $Cr_2Ge_2Te_6$/NiO, the critical thickness (t_C) below which the T_C starts to decrease is smaller (∼7 nm), and the MOKE hysteresis cannot be observed for ∼4 nm or thinner. For $Cr_2Ge_2Te_6$ without any overlayer, t_C is even smaller [3]. The difference in t_C can be related to the different amount of "dead layers" (disordered or degraded layers below the $Cr_2Ge_2Te_6$ top surface). These dead layers can weaken the magnetism, and lessen the enhanced magnetism induced by strain in thin flakes. The smaller t_C for $Cr_2Ge_2Te_6$/NiO may be attributed to the relatively thinner degraded region (dead layers) compared to $Cr_2Ge_2Te_6$/MgO. Indeed, we observed modified Raman spectra, with strong oxide-related peaks dominating the Raman spectra, of $Cr_2Ge_2Te_6$/MgO flakes when the thickness of $Cr_2Ge_2Te_6$ is below ∼12 nm, whereas such modified spectra are observed for flakes with $Cr_2Ge_2Te_6$ thickness below ∼4 nm for $Cr_2Ge_2Te_6$/NiO samples. These thickness values match those below which we could no longer observe magnetic hysteresis and may be taken as an estimated thickness of the degraded region of dead layers. In the case of $Cr_2Ge_2Te_6$/NiO, the ∼4-nm-thick degraded region is also consistent with the thickness of intermixing region (L_1, Fig. 4). In summary, while the enhanced magnetism can be observed not only with NiO but also with other overlayer materials (such as MgO) that can induce strain, different overlayer films can give different interfaces with $Cr_2Ge_2Te_6$ that affect the $Cr_2Ge_2Te_6$ thickness dependence of the enhanced ferromagnetism.

In conclusion, we demonstrated a method to induce strain or artificially stretch the lattice in a crystalline $Cr_2Ge_2Te_6$ flake, by inducing wrinkles after depositing an overlayer material such as NiO or MgO. We experimentally characterized the local magnetic and lattice properties, established the relationship with local strain, and corroborated our results with theoretical calculations. Our work provides an easily implementable method (via heterointerfaces) for strain engineering that could apply to a wide variety of 2D vdW materials (and even non-2D materials), to control the electronic, magnetic, and optical properties and develop new functionalities.

This work was supported in part (materials development, other measurements, analysis, and computation) by AIMR and its "fusion" research program, under World Premier International Research Center Initiative (WPI), the Ministry of Education, Culture, Sports, Science and Technology (MEXT), Japan, and by Grant-in-Aid for Scientific Research, Japan Society for the Promotion of Science KAKENHI (Grants No. 20K14399, No. 22H01896, and No. 23K03293), and JST-CREST (Grant No. JPMJCR18T1). This work was also supported in part (Raman and MOKE measurements) by the Quantum Science Center, a Department of Energy National Quantum Information Science Center. We also acknowledge the partial support of National Science Foundation (EFMA Award No. 1641101 and ECCS Award No. 1711332) for earlier phases (materials development and strain engineering) of this work.

[1] C. Gong, L. Li, Z. Li, H. Ji, A. Stern, Y. Xia, T. Cao, W. Bao, C. Wang, Y. Wang, Z. Q. Qiu, R. J. Cava, S. G. Louie, J. Xia, and X. Zhang, Discovery of intrinsic ferromagnetism in two-dimensional van der Waals crystals, Nature (London) **546**, 265 (2017).

[2] B. Huang, G. Clark, E. Navarro-Moratalla, D. R. Klein, R. Cheng, K. L. Seyler, D. Zhong, E. Schmidgall, M. A. McGuire, D. H. Cobden, W. Yao, D. Xiao, P. Jarillo-Herrero, and X. Xu, Layer-dependent ferromagnetism in a van der Waals crystal down to the monolayer limit, Nature (London) **546**, 270 (2017).

[3] C. Gong and X. Zhang, Two-dimensional magnetic crystals and emergent heterostructure devices, Science **363**, eaav4450 (2019).

[4] Y. Tian, M. J. Gray, H. Ji, R. Cava, and K. S. Burch, Magneto-elastic coupling in a potential ferromagnetic 2D atomic crystal, 2D Mater. **3**, 025035 (2016).

[5] J.-U. Lee, S. Lee, J. H. Ryoo, S. Kang, T. Y. Kim, P. Kim, C.-H. Park, J.-G. Park, and H. Cheong, Ising-type magnetic ordering in atomically thin $FePS_3$, Nano Lett. **16**, 7433 (2016).

[6] Y. Deng, Y. Yu, Y. Song, J. Zhang, N. Z. Wang, Z. Sun, Y. Yi, Y. Z. Wu, S. Wu, J. Zhu, J. Wang, X. H. Chen, and Y. Zhang, Gate-tunable room-temperature ferromagnetism in two-dimensional Fe_3GeTe_2, Nature (London) **563**, 94 (2018).

[7] Z. Wang, T. Zhang, M. Ding, B. Dong, Y. Li, M. Chen, X. Li, J. Huang, H. Wang, X. Zhao, Y. Li, D. Li, C. Jia, L. Sun, H. Guo, Y. Ye, D. Sun, Y. Chen, T. Yang, J. Zhang, S. Ono, Z. Han, and Z. Zhang, Electric-field control of magnetism in a few-layered van der Waals ferromagnetic semiconductor, Nat. Nanotechnol. **13**, 554 (2018).

[8] T. Song, Z. Fei, M. Yankowitz, Z. Lin, Q. Jiang, K. Hwangbo, Q. Zhang, B. Sun, T. Taniguchi, K. Watanabe, M. A. McGuire, D. Graf, T. Cao, J.-H. Chu, D. H. Cobden, C. R. Dean, D. Xiao, and X. Xu, Switching 2D magnetic states via pressure tuning of layer stacking, Nat. Mater. **18**, 1298 (2019).

[9] J. Cenker, S. Sivakumar, K. Xie, A. Miller, P. Thijssen, Z. Liu, A. Dismukes, J. Fonseca, E. Anderson, X. Zhu, X. Roy, D. Xiao, J.-H. Chu, T. Cao, and X. Xu, Reversible strain-induced magnetic phase transition in a van der Waals magnet, Nat. Nanotechnol. **17**, 256 (2022).

[10] H. Idzuchi, A. E. Llacsahuanga Allcca, X. C. Pan, K. Tanigaki, and Y. P. Chen, Increased Curie temperature and enhanced perpendicular magneto anisotropy of $Cr_2Ge_2Te_6$/NiO heterostructures, Appl. Phys. Lett. **115**, 232403 (2019).

[11] T. Peña, S. A. Chowdhury, A. Azizimanesh, A. Sewaket, H. Askari, and S. M. Wu, Strain engineering 2D MoS_2 with thin film stress capping layers, 2D Mater. **8**, 045001 (2021).

[12] See Supplemental Material at http://link.aps.org/supplemental/10.1103/PhysRevB.111.L020402 for the characterization of the wrinkle structure, the details of experimental procedure, the Raman analysis of bending $Cr_2Ge_2Te_6$ samples on PET flexible substrates, the correlation of Raman peaks E_g^1 and A_{1g}^2, the details of the polarized Raman measurements, the DFT calculation details, the analysis procedure for Figs. 4(b) and 4(c) and, the MOKE measurements of $Cr_2Ge_2Te_6$/MgO. The Supplemental Material also contains Refs. [13–22].

[13] Y. Liu, W. Wang, H. Lu, Q. Xie, L. Chen, H. Yin, G. Cheng, and X. Wu, The environmental stability characterization of exfoliated few-layer $CrXTe_3$ (X = Si, Ge) nanosheets, Appl. Surf. Sci. **511**, 145452 (2020).

[14] R. Loudon, The Raman effect in crystals, Adv. Phys. **50**, 813 (2001).

[15] G. Kresse and J. Hafner, *Ab initio* molecular dynamics for liquid metals, Phys. Rev. B **47**, 558 (1993).

[16] G. Kresse and J. Furthmüller, Efficiency of *ab-initio* total energy calculations for metals and semiconductors using a plane-wave basis set, Comput. Mater. Sci. **6**, 15 (1996).

[17] G. Kresse and J. Furthmüller, Efficient iterative schemes for *ab initio* total-energy calculations using a plane-wave basis set, Phys. Rev. B **54**, 11169 (1996).

[18] J. P. Perdew, K. Burke, and M. Ernzerhof, Generalized gradient approximation made simple, Phys. Rev. Lett. **77**, 3865 (1996).

[19] G. Kresse and D. Joubert, From ultrasoft pseudopotentials to the projector augmented-wave method, Phys. Rev. B **59**, 1758 (1999).

[20] R. F. L. Evans, U. Atxitia, and R. W. Chantrell, Quantitative simulation of temperature-dependent magnetization dynamics and equilibrium properties of elemental ferromagnets, Phys. Rev. B **91**, 014425 (2015).

[21] A. Nakata, J. S. Baker, S. Y. Mujahed, J. T. L. Poulton, S. Arapan, J. Lin, Z. Raza, S. Yadav, L. Truflandier, T. Miyazaki, and D. R. Bowler, Large scale and linear scaling DFT with the CONQUEST code, J. Chem. Phys. **152**, 164112 (2020).

[22] Z. Li, Y. Lv, L. Ren, J. Li, L. Kong, Y. Zeng, Q. Tao, R. Wu, H. Ma, B. Zhao, D. Wang, W. Dang, K. Chen, L. Liao, X. Duan, X. Duan, and Y. Liu, Efficient strain modulation of 2D materials via polymer encapsulation, Nat. Commun. **11**, 1151 (2020).

[23] A. Castellanos-Gomez, R. Roldán, E. Cappelluti, M. Buscema, F. Guinea, H. S. J. van der Zant, and G. A. Steele, Local strain engineering in atomically thin MoS_2, Nano Lett. **13**, 5361 (2013).

[24] N. Matuda, S. Baba, and A. Kinbara, Internal stress, young's modulus and adhesion energy of carbon films on glass substrates, Thin Solid Films **81**, 301 (1981).

[25] T. M. G. Mohiuddin, A. Lombardo, R. R. Nair, A. Bonetti, G. Savini, R. Jalil, N. Bonini, D. M. Basko, C. Galiotis, N. Marzari, K. S. Novoselov, A. K. Geim, and A. C. Ferrari, Uniaxial strain in graphene by Raman spectroscopy: *G* peak splitting, Grüneisen parameters, and sample orientation, Phys. Rev. B **79**, 205433 (2009).

[26] Y. Ga, Q. Cui, J. Liang, D. Yu, Y. Zhu, L. Wang, and H. Yang, Dzyaloshinskii-Moriya interaction and magnetic skyrmions induced by curvature, Phys. Rev. B **106**, 054426 (2022).

[27] B. H. Zhang, Y. S. Hou, Z. Wang, and R. Q. Wu, First-principles studies of spin-phonon coupling in monolayer $Cr_2Ge_2Te_6$, Phys. Rev. B **100**, 224427 (2019).

[28] W. Ge, K. Xu, W. Xia, Z. Yu, H. Wang, X. Liu, J. Zhao, X. Wang, N. Yu, Z. Zou, Z. Yan, L. Wang, M. Xu, and Y. Guo, Raman spectroscopy and lattice dynamical stability study of 2D ferromagnetic semiconductor $Cr_2Ge_2Te_6$ under high pressure, J. Alloys Compd. **819**, 153368 (2020).

[29] Y. Sun, R. C. Xiao, G. T. Lin, R. R. Zhang, L. S. Ling, Z. W. Ma, X. Luo, W. J. Lu, Y. P. Sun, and Z. G. Sheng, Effects of hydrostatic pressure on spin-lattice coupling in two-dimensional ferromagnetic $Cr_2Ge_2Te_6$, Appl. Phys. Lett. **112**, 072409 (2018).

[30] V. Carteaux, D. Brunet, G. Ouvrard, and G. Andre, Crystallographic, magnetic and electronic structures of a new layered ferromagnetic compound $Cr_2Ge_2Te_6$, J. Phys.: Condens. Matter **7**, 69 (1995).

[31] A. V. Ushakov, D. A. Kukusta, A. N. Yaresko, and D. I. Khomskii, Magnetism of layered chromium sulfides $MCrS_2$ (M = Li, Na, K, Ag, and Au): A first-principles study, Phys. Rev. B **87**, 014418 (2013).

[32] X.-J. Dong, J.-Y. You, Z. Zhang, B. Gu, and G. Su, Great enhancement of Curie temperature and magnetic

anisotropy in two-dimensional van der Waals magnetic semiconductor heterostructures, Phys. Rev. B **102**, 144443 (2020).

[33] Q. Cui, J. Liang, Z. Shao, P. Cui, and H. Yang, Strain-tunable ferromagnetism and chiral spin textures in two-dimensional Janus chromium dichalcogenides, Phys. Rev. B **102**, 094425 (2020).

[34] Y. Wang, C. Wang, S.-J. Liang, Z. Ma, K. Xu, X. Liu, L. Zhang, A. S. Admasu, S.-W. Cheong, L. Wang, M. Chen, Z. Liu, B. Cheng, W. Ji, and F. Miao, Strain-sensitive magnetization reversal of a van der Waals magnet, Adv. Mater. **32**, 2004533 (2020).

[35] We characterized $Cr_2Ge_2Te_6$/NiO where $Cr_2Ge_2Te_6$ is in a form of flake or bulk. The bulk case also shows consistent results.

[36] K. Momma and F. Izumi, VESTA 3 for three-dimensional visualization of crystal, volumetric and morphology data, J. Appl. Crystallogr. **44**, 1272 (2011).